



PERGAMON

Deep-Sea Research I 49 (2002) 1551–1569

DEEP-SEA RESEARCH  
PART I

www.elsevier.com/locate/dsr

# Modelling the seasonal cycle of the exchange flow in Bab El Mandab (Red Sea)

Mark Siddall<sup>a,\*</sup>, David A. Smeed<sup>a</sup>, Stephan Matthiesen<sup>b</sup>, Eelco J. Rohling<sup>a</sup>

<sup>a</sup>Southampton Oceanography Centre, European Way, Southampton, SO14 3ZH, UK

<sup>b</sup>Institute for Meteorology, The University of Edinburgh, Edinburgh, UK

Received 24 November 2001; received in revised form 19 March 2002; accepted 11 June 2002

## Abstract

A minimum complexity, three-layer hydraulic model has been further developed to simulate the seasonal cycle of the exchange flow in Bab el Mandab (Red Sea). Unlike earlier versions our model incorporates a realistic channel cross-section. To a good approximation the model simulates observed fluxes through the strait and the layer depths at Hanish Sill. The model results indicate that the summertime intrusion of Gulf of Aden Intermediate Water into the Red Sea has been a robust feature of the exchange for the last 10 500 years. The modern intrusion acts as a dynamic barrier to the exchange in the upper and lower layers effectively, reducing the mean annual flux in each layer by 26% and 33% compared to model runs without the intrusion.

© 2002 Elsevier Science Ltd. All rights reserved.

*Keywords:* Hydraulic control; Critical flow; Three-layer exchange; Indian Ocean; Strait

## 1. Introduction

### 1.1. The Red Sea

The Red Sea is a long narrow basin connected to the Gulf of Aden (Indian Ocean) at its southerly extreme via Bab el Mandab. The basin is 2000 km long but only 280 km wide (Morcos, 1970), extending from 30°N to 12.5°N. The central channel reaches depths of 2000 m but the average depth of the Red Sea is only 450 m (Degens and Ross, 1969). This central channel is fringed in the southern Red Sea by shallow shelves less than 50 m

deep (Fig. 1). To the north lie the Gulf of Suez and the Gulf of Aqaba.

The shallowest section of Bab el Mandab consists of Hanish sill, close to Hanish Islands, and is located 150 km to the north of the narrowest passage near Perim Island. The greatest depth at the sill is 137 m (Fig. 1) and the total width of the sill section is about 110 km (Werner and Lange, 1975). The sill depth maximum occurs within a deep passage that is only 6 km wide, outside of which the depth is only of the order of 50 m (Murray and Johns, 1997) (Fig. 3). The total width at the Perim Narrows is only about 18 km (Murray and Johns, 1997) with a depth of about 300 m in the central channel (Maillard and Soliman, 1986) (Fig. 3).

\*Corresponding author. Fax: +44-23-8059-3059.

E-mail address: ms14@soc.soton.ac.uk (M. Siddall).

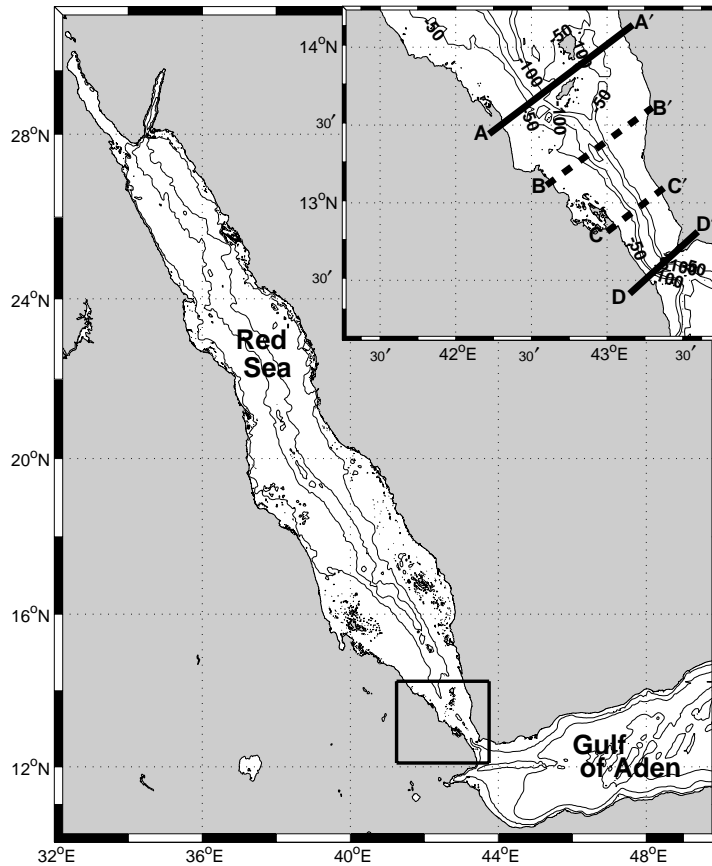


Fig. 1. Map of the Red Sea including a detailed projection of the Bab el Mandab Strait (top right). The letters mark the transects used for the cross-sections in Fig. 3. AA' is at Hanish Sill and DD' is at Perim Narrows.

High evaporation and low precipitation and run-off result in a net freshwater loss of  $2 \text{ m yr}^{-1}$  over the Red Sea (Morcos, 1970). More recent and precise estimates put the net annual average evaporation at  $2.06 \pm 0.22 \text{ m yr}^{-1}$  (Sofianos et al., 2002). This is the major contributor to the net buoyancy loss in the Red Sea of  $2 \times 10^{-8} \text{ m}^2 \text{ s}^{-1}$  (Tragou et al., 1999). The buoyancy loss within the basin is responsible for the creation of Red Sea Water (RSW) throughout the basin. RSW lies above Red Sea Deep Water (RSDW). The deeper RSDW is formed by intense wintertime evaporation over the Gulf of Suez and the Gulf of Aqaba (Maillard and Soliman, 1986; Cember, 1988).

RSW and RSDW are observed to flow out of the Red Sea at Bab el Mandab throughout the year (Pratt et al., 1999, 2000). Between November and early June (winter regime) this outflow is balanced simply by an inflow of Gulf of Aden Surface Water (GASW). From June to October the south-west monsoon winds provoke an upwelling of Gulf of Aden Intermediate Water (GAIW) to the south of the straits (Smeed, 1997). This intermediate layer moves towards the Red Sea as it is upwelled. The flux of GAIW towards the Red Sea eventually becomes greater than the outflow of RSW and RSDW. The winter surface inflow of GASW is forced to reverse in order to balance the

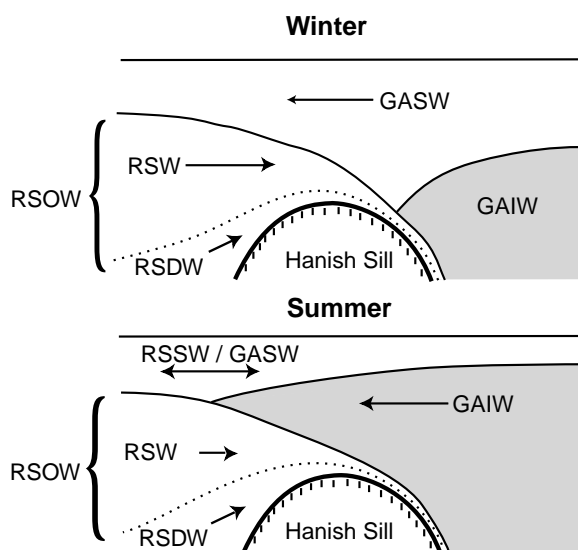


Fig. 2. Schematic of the summer and winter exchange regimes. GASW is Gulf of Aden Surface Water, GAIW is Gulf of Aden Intermediate Water, RSSW is Red Sea Surface Water, RSW is Red Sea Water, RSDW is Red Sea Deep Water and RSOW is Red Sea Overflow Water (RSW + RSDW). Note that during the summer regime the upper layer inflow of GASW reverses to become RSW. Also the GAIW layer thins and widens as it emerges into the Red Sea so that at 18°N it disappears from observations (Smeed, 1997).

inflowing GAIW (Fig. 2) (Smeed, 1997, 2000; Sofianos et al., 2002). In this paper we attempt to model this seasonality quantitatively by the approach outlined below.

### 1.2. Exchange models

The hydraulic control of density-driven flows at sea straits has been studied in many locations (e.g. the Bosphorus Strait, Lane-Serff et al., 1997; the Vema Channel, Hogg, 1983). Most notably the Strait of Gibraltar, at the entrance to the Mediterranean, has been considered in some depth starting with a paper by Bryden and Stommel (1984) and most recently with a paper by Bryden et al. (1994). Assuming a two-layer flow, Bryden et al. (1994) used a maximal exchange hypothesis combined with the Knudsen equations (Nielsen, 1912) for freshwater and salt conservation in the Mediterranean basin to calculate the exchange

fluxes for Mediterranean Water and Atlantic Water. By including the effects of bottom friction and realistic channel cross section, they could calculate the fluxes to a good approximation of their observed values. Bormans et al. (1986) question the validity of the maximal exchange hypothesis and consider the annual cycle in Mediterranean exchange. Their results suggest that the exchange may be sub-maximal for part of the year.

Smeed (2000) attempted to model the seasonally varying two/three-layer annual exchange cycle in the Red Sea. His work effectively generates the annual cycle in a qualitative sense, but it overestimates the fluxes by a factor of two. Smeed (2000) suggested that this poor quantitative reproduction of observations may result from the unrealistic rectangular bathymetry used in the model, since Bryden and Kinder (1991) had found that realistic bathymetry affected the calculated fluxes (in their case in the Mediterranean) by a factor of three.

Here we aim to expand upon the three-layer Bernoulli functional approach used by Smeed (2000) by including realistic bathymetry. The results are validated by comparison with fluxes calculated by Sofianos et al. (2002). The model has been developed in order to consider various scenarios for the Red Sea circulation put forward by the paleoceanographic community (Winter et al., 1983; Rohling, 1994; Rohling and Zachariasse, 1996; Fenton, 1998; Rohling et al., 1998; Fenton et al. 2000). These will be considered in the discussion section.

## 2. Method

### 2.1. Defining the problem

For a thorough review of hydraulic control models we refer to the study of Lane-Serff et al. (2000). Here we use a hydraulic model with a realistic strait morphology to determine the strait fluxes and interface depths at the sill as a function of the evaporation over the Red Sea, the reduced gravity and, most significantly, the interface

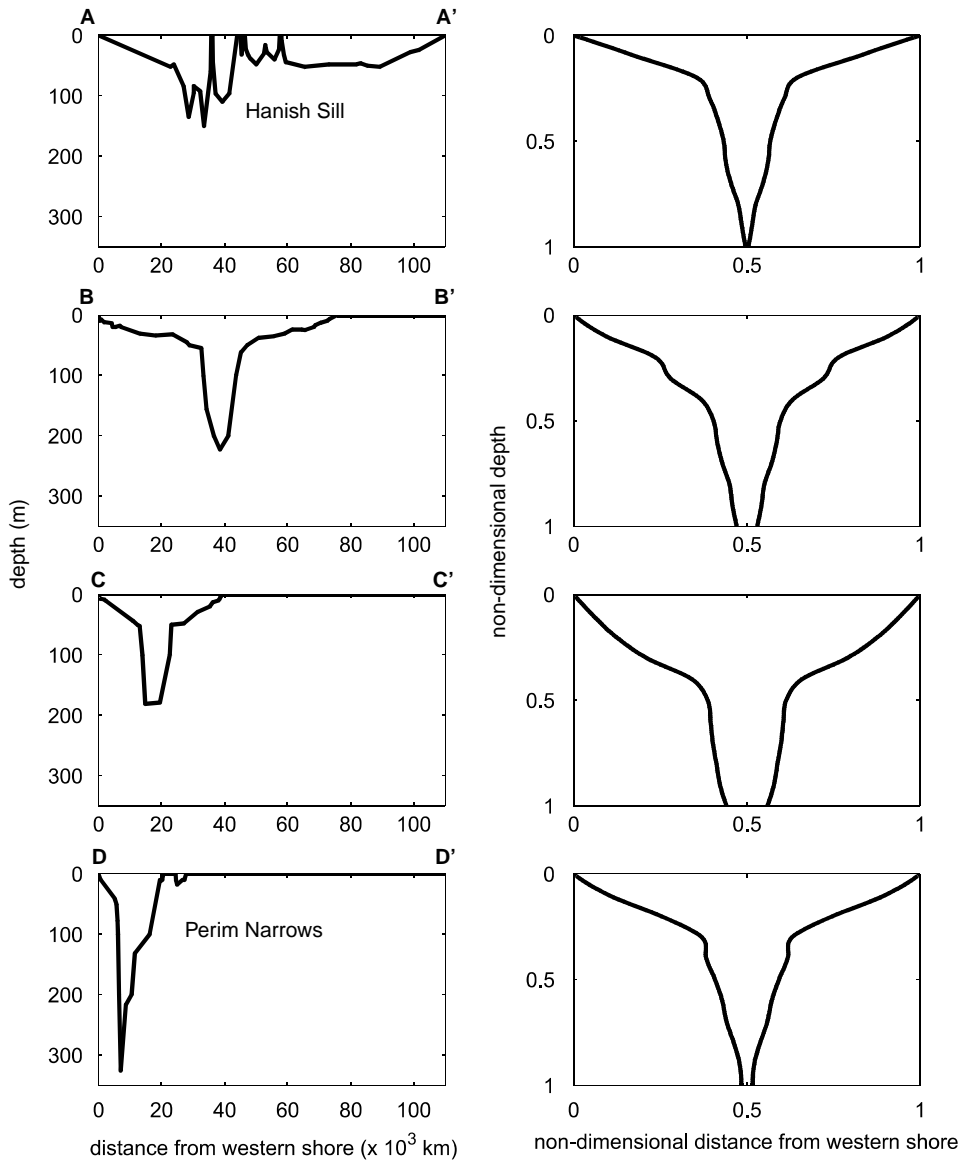


Fig. 3. Channel cross-sections at the transects marked on Fig. 1 (left hand column). Channel width versus depth normalised to the surface width and maximum cross-sectional depth for the sections shown in the left hand column, plotted symmetrically (right hand column).

heights in the reservoirs at either end of the strait, for a realistic strait morphology.

2.2. Configuration

The present model consists of two reservoirs of infinite depth and width joined by a channel of

uniform, finite width and non-rectangular cross section. The channel shallows to a minimum depth at the sill.

To establish the fundamental distribution of width with depth of the channel four cross sections were taken along Bab el Mandab (Figs. 1 and 3). These cross-sections were non-dimensionalised

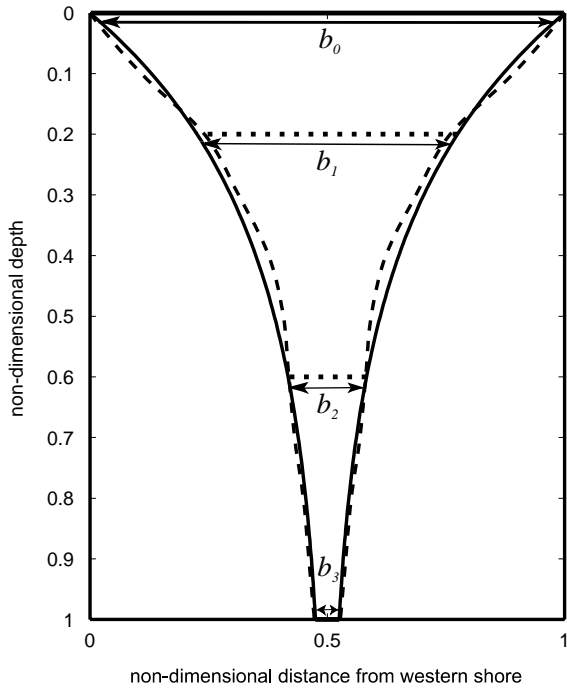


Fig. 4. The mean channel width against depth calculated from the transects shown in the right hand column of Fig. 3 (----) and the best fit of the exponential function (1) (—) plotted symmetrically.  $b_0$ ,  $b_1$ ,  $b_2$  and  $b_3$  are the non-dimensional channel width at the surface, water mass and bottom interfaces (· · · · ·).

with respect to the maximum depth ( $D$ ) and surface width ( $B$ ) of the channel at each transect. A mean could then be generated for the non-dimensional widths at respective depths (Fig. 4). This process inevitably smooths any sharp changes in the bottom slope, but the important features of the four cross sections are preserved (compare Figs. 3 and 4). Eq. (1) gives the width of the channel with respect to depth.

$$b(z) = \exp(kz), \tag{1}$$

where  $b$  is the non-dimensional width of the channel and  $z$  is the non-dimensional depth. The constant  $k$  in the exponential function (1) is least squares fitted to the curve of width against depth (Fig. 4). The value of  $k$  used in the model is  $3.0 \pm 0.2$ .

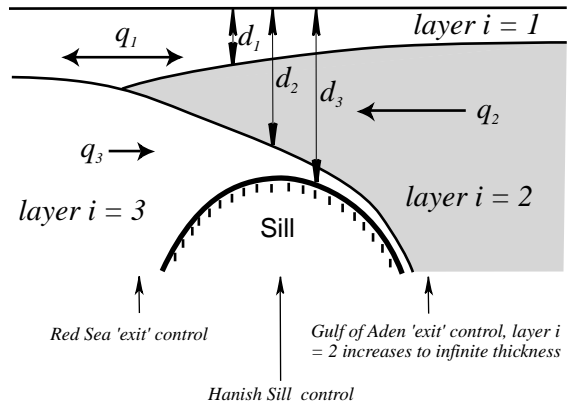


Fig. 5. Model variables (see text for details).

Integrating across the  $i$ th layer from  $z = d_{i-1}$  to  $d_i$  gives  $a_i$ , the non-dimensional cross sectional area of layer  $i$ . The subscript  $i$  represents the layer number ( $i = 1 \rightarrow 3$  starting from the upper layer),  $d_i$  is the non-dimensional depth of the interface below layer  $i$ , and  $a_i$  is the non-dimensional cross sectional area of layer  $i$  (see Figs. 4 and 5 for definitions). Thus

$$a_i = \left(\frac{1}{k}\right) (\exp(kd_i) - \exp(kd_{i-1})). \tag{2}$$

Tests of sensitivity to the parameter  $k$  can be easily carried out. Using piecewise-linear bathymetry made little difference to our results. For the purposes of obtaining dimensional model results we used the surface width of the strait at the sill,  $B_S$  (110 km) and the maximum depth at the sill,  $H_S$  (137 m) to re-dimensionalise the cross-sectional area. The depth can be extended to infinity at the ‘exits’ with this formalism.

As in previous studies of the Red Sea (Smeed, 1997, 2000) and the Mediterranean (Bryden and Kinder, 1991; Bryden et al., 1994), the outflowing layers RSW and RSDW are taken as one, uniform layer, from now on denoted as Red Sea Overflow Water (RSOW) (i.e. RSOW = RSW + RSDW), which thins to a very small (zero) thickness in the Gulf of Aden. We also assume that the summer inflowing GAIW layer reduces to zero thickness in the Red Sea. These assumptions simplify the

solution process since the number of interface heights is thus reduced from four to two (one for each basin). Finally the model is quasi-steady; it is always at equilibrium with respect to the driving parameters used to generate the given solution at a given time.

### 2.3. Bernoulli functionals

The approach used is to conserve the Bernoulli energy along the strait. Lane-Serff et al. (2000) derive the generalised Bernoulli functionals (3) for many layers, using the three-layer case as a specific example, and we refer to that study for the detailed derivations. In the three-layer case the relevant Bernoulli functionals are

$$\begin{aligned} \frac{1}{2} \left( \frac{Q_1}{A_1} \right)^2 - \frac{1}{2} \left( \frac{Q_2}{A_2} \right)^2 + g'_1 D_1 &= H'_1, \\ \frac{1}{2} \left( \frac{Q_2}{A_2} \right)^2 - \frac{1}{2} \left( \frac{Q_3}{A_3} \right)^2 + g'_2 (D_1 + D_2) &= H'_2. \end{aligned} \quad (3)$$

where  $Q$  is the flux in a given layer (subscripts 1, 2, and 3 denote the upper, middle and lower layer respectively),  $A$  is the cross-sectional area of that layer,  $D$  is the interface depth below a given layer and  $H'$  is the Bernoulli constant for the interface. The reduced gravity,  $g'$ , of the interface is given by  $g'_i = 2g(\rho_i + 1 - \rho_i)/\bar{\rho}$ , where  $\rho$  stands for the density and  $\bar{\rho}$  is the mean density of all the layers. Unless stated explicitly upper case letters denote dimensional numbers and lower case letters denote their non-dimensional counterparts (Fig. 5 gives the definitions for the non-dimensional symbols used in the equations).

The Bernoulli functionals (3) assume an inviscid, hydrostatic and Boussinesq fluid in three discrete layers beneath a rigid lid. Since any changes in strait width are small compared to along-strait distance, the flow may be assumed to be uni-directional within each layer. The flow is assumed to be non-rotating. Averaged over an annual cycle and assuming no interannual variability, mass is conserved. However, at any particular instant during the annual cycle the mass of the Red Sea will be varying. Here we make the approximation of a balanced volume budget, so that  $Q_1 + Q_2 + Q_3 + E = 0$ , where  $E$  is the net

evaporative flux from the Red Sea basin. While the annual volume budget of the Red Sea balances, satellite altimetric observations indicate some seasonal variation in the basin volume, which is not accounted for in the model (Cromwell and Smeed, 1998).

For the purposes of the model the variables are non-dimensionalised by  $B_S$  and  $D_S$  (the surface width and maximum depth of the channel at the sill) and the total reduced gravity  $g' = g'_1 + g'_2$ . The precise non-dimensionalisations are

$$\begin{aligned} D_i &= D_S d_i, \quad B_i = B_S b_i, \quad g'_1 = r g', \quad A_i = a_i A_S, \\ H'_i &= g' D_S H_i, \quad Q_i = A_S (g' D_S)^{1/2} q_i, \\ g'_2 &= (1 - r) g'. \end{aligned} \quad (4)$$

The subscript S denotes values for the sill. The parameter  $r = (\rho_2 - \rho_1)/(\rho_3 - \rho_1)$  can vary between 0 and 1 (see Fig. 5 for definitions). The non-dimensional Bernoulli functionals,  $J$  and  $K$ , are

$$J = \frac{1}{2} \left( \frac{q_1}{a_1} \right)^2 - \frac{1}{2} \left( \frac{q_2}{a_2} \right)^2 + r d_1 - H_1 = 0, \quad (5)$$

$$K = \frac{1}{2} \left( \frac{q_2}{a_2} \right)^2 - \frac{1}{2} \left( \frac{q_3}{a_3} \right)^2 + d_2 (1 - r) - H_2 = 0. \quad (6)$$

There are multiple solutions to the Bernoulli equations. The correct solution for each part of the channel is determined by the driving parameters, and to complete the solution it is necessary to consider the control points.

A control is defined as a point downstream from which the flow is such that one or more of the internal wave modes are swept downstream and cannot communicate with the upstream reservoir. Maximal exchange occurs when none of the possible internal wave modes can propagate between basins and the geometry of the strait controls the exchange. It can also be shown that the solution to (5) and (6) switches branch at a control (Smeed, 2000). This condition is analogous to a Froude number of unity in a single layer hydraulic flow (Gill, 1977). In three layers with

non-uniform cross section the control condition is

$$F_2^2 \left( F_2^2 \frac{b_1}{b_2} \right) - \left( r - F_1^2 - F_2^2 \frac{b_1}{b_2} \right) \times \left( 1 - r - F_2^2 - F_3^2 \frac{b_2}{b_3} \right) = 0. \quad (7)$$

We define  $F_i$  as the layer Froude number, where  $F_i^2 = b_i q_i^2 / a_i^3$ . The control condition (7) is derived in Appendix A.

The regularity condition requires that the solution at the control is realisable (Dalziel, 1991). Given basins of infinite depth and width, connected by a channel with parallel sides, the regularity condition can be satisfied, and hence controls exist, only at the sill or either of the two ‘exits’ (Killworth, 1992). Thus the simplification of parallel isobaths allows us to determine the location of the controls, and so the degrees of freedom (unknowns) in the problem are reduced. In reality the ‘exit’ controls move along the strait as a function of the driving parameters of the flow (Smeed, 2000).

If hydraulic control occurs in a flow there must also be a hydraulic jump, because the flow in the reservoirs is sub-critical. When control occurs we assume that hydraulic jumps are present, but we do not calculate them explicitly. The only condition applied is that energy is lost at the hydraulic jump. Note that if the intermediate layer is not present the equations are identical to those for the two-layer case (Dalziel, 1991).

In summary, there are a total of eight Eqs. (B.1)–(B.8) (Appendix B); the Bernoulli functionals and control conditions for both ‘exits’ and the sill. A number of different solution types are possible. For each type a different subset of the equations must be solved. The solution type is determined by the forcing parameters. A full discussion is given in Smeed (2000).

#### 2.4. Drivers

The modelled annual cycle is driven by four external parameters, which are known to varying degrees of certainty. These are: the net evaporative flux over the basin, the relative gravity, and the

layer depths of the upper interface in the Red Sea and Gulf of Aden.

To estimate the annual mean evaporation over the Red Sea Sofianos et al. (2002) did not use their estimate of the volume fluxes directly because their error in the measurement of the upper layer flux was large. Instead they assumed annual conservation of salt within the Red Sea so that they could diagnose the mean flux in the upper layer. To calculate the monthly mean evaporation, conservation of salt cannot be assumed (Smeed, 1997). We therefore calculated the mean monthly evaporative flux by volume conservation in the basin ( $E = Q_1 + Q_2 + Q_3$ ) using the observations of Sofianos et al. (2002). This gives the annually integrated flux as  $2.1 \text{ m yr}^{-1}$ , which compares with their diagnosed integrated flux of  $2.06 \pm 0.22 \text{ m yr}^{-1}$ . The monthly mean evaporative flux over the basin calculated in this way has a maximum of  $2.8 \pm 0.22 \text{ m yr}^{-1}$  in mid-winter and a minimum of  $1.4 \pm 0.22 \text{ m yr}^{-1}$  in mid-summer (Fig. 6). We use the same uncertainty ( $\pm 0.22 \text{ m yr}^{-1}$ ) as Sofianos et al. (2002).

The question arises as to whether to use values for  $r$  generated in the reservoirs or in the strait. Our model is inviscid and therefore ignores any mixing that may occur in the strait, so we chose the value of  $r$  generated from the reservoir conditions. The reduced gravity used is therefore essentially the same as that cited in Smeed’s (2000) model: The reduced gravity for the lower interface  $g'_2$  is constant throughout the year (Smeed, 1997), so the ratio of the density change across the upper interface to the density change across the two interfaces,  $r$ , varies almost uniquely with  $g'_1$ . Furthermore the salinity in the upper layer varies little throughout the year (Sofianos et al., 2002) so that the variation in  $g'_1$  is due almost entirely to warming/cooling of the surface layer. To generate an annual cycle for  $r$  we used the temperatures for the surface layer quoted in Sofianos et al. (2002). All other temperature and salinity values are taken from Smeed (1997). The Sofianos et al. (2002) integrated upper layer temperature in the strait will not be identical to the reservoir condition because of mixing in the strait. Despite this we consider the Sofianos et al. (2002) record to be the best one to use to generate the annual cycle of  $r$ .

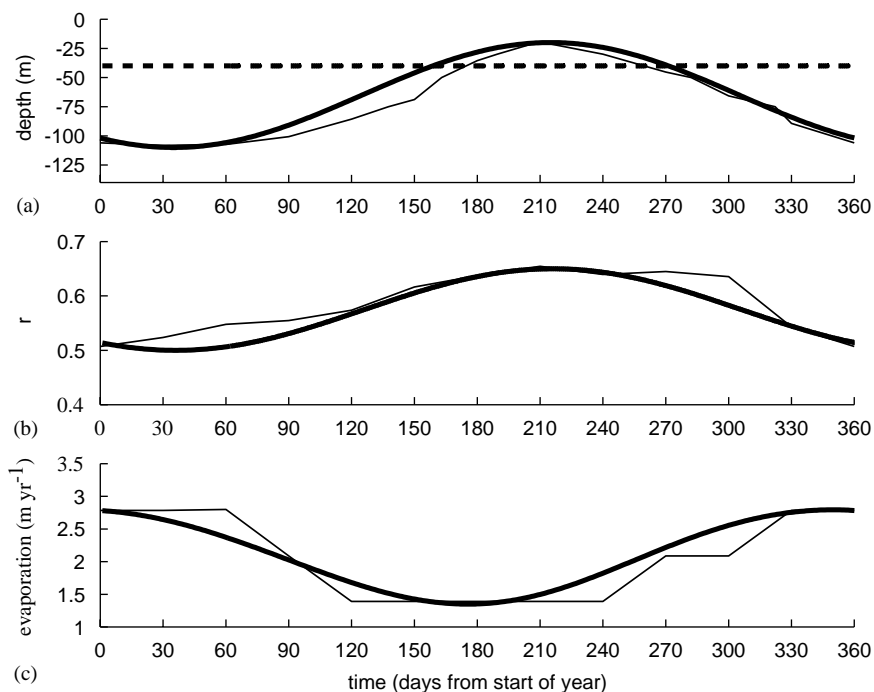


Fig. 6. Forcing parameters used in the model (heavy lines). Light lines represent observed values (see text for details).

The upper layer temperatures quoted in Sofianos et al. (2002) are similar to those quoted in Smeed (1997). A value of  $r = 0.5 \pm 0.06$  is found in mid-winter, which increases to  $r = 0.65 \pm 0.06$  in mid-summer when the surface layer is warmed. This compares to  $r = 0.5$  in winter and  $r = 0.67$  in summer from Smeed (1997). The evaporative flux and  $r$  are made to vary sinusoidally with maxima in January and July respectively (Fig. 6).

The interfaces that must be chosen are the upper interface in the Gulf of Aden, which is between GASW and GAIW, and the upper interface in the Red Sea, which is between RSSW/GASW and RSOW (Fig. 2). These interfaces represent the base of the upper layer in each reservoir. The choice of interface depths is complicated, since the actual exchange takes place in a gradually stratified flow, rather than in the idealised discrete layers used by the model. Pratt et al. (1999, 2000) have made monthly mean current meter readings at the Hanish Sill and Perim Narrows. The zero velocity

crossings of their interpolated profiles can be matched to an isopycnal that is traceable into both the Red Sea and the Gulf of Aden. This isopycnal is effectively the base of the upper layer. The velocity zero crossing, which represents the base of the upper layer, occurs at an isopycnal of  $1024.7 \text{ kg cm}^{-3}$ . The interface depth used in the Gulf of Aden (i.e. the interface between RSSW or GASW and GAIW) is given by the depth of this isopycnal in the Gulf from Levitus data, and varies approximately sinusoidally between  $20 \pm 5 \text{ m}$  in mid-July and  $110 \pm 5 \text{ m}$  in March (Fig. 6). The  $1024.7 \text{ kg cm}^{-3}$  isopycnal falls towards the centre of the pycnocline in the Red Sea and the Gulf of Aden. Large changes in the chosen density of the pycnocline value for the interface relate to small changes in interface depth. For the purposes of the model we fit an idealised sine curve to this signal with a maximum in mid-July (Fig. 6).

The coverage of Levitus data in the Red Sea is too low to be used to generate similar values in the

Red Sea. However, we note that the zero crossing in the Pratt et al. (1999, 2000) data does not vary much from a value of  $\sim 50$  m during the winter months. Over the winter period the two-layer exchange is predominantly forced by the interface depth in the Red Sea so either the appropriate interface height varies little or the exchange is maximal. We also note that during this period the depth of the interface in the Red sea must be less than that at the sill unless the exchange is maximal (i.e.  $< 50$  m). The  $1024.7 \text{ kg cm}^{-3}$  isopycnal resides at approximately  $40 \pm 5$  m depth in the June observations of Neuman and McGill (1962). Maillard and Soliman's (1986) October observations are disrupted by the presence of a meso-scale eddy but still show the  $1024.7 \text{ kg cm}^{-3}$  isopycnal at about the same depth of  $\sim 40 \pm 5$  m. The Red Sea interface depth is therefore taken at a constant depth of  $40 \pm 5$  m (Fig. 6). Because this isopycnal falls within the pycnocline, a large change in density equates to only a small change in depth. This definition of the interface heights in the reservoirs is therefore not very sensitive to which isopycnal is chosen.

### 3. Results

#### 3.1. Comparison of model with observations

Given the values for the net evaporative flux, interface depths, and  $r$  mentioned above, the model was evaluated for the annual range of parameter values at intervals of one day. Maximum and minimum seasonal flux cycles were generated within the range of uncertainties for the net evaporative flux, interface depths, and  $r$ . These are shown alongside the model result for the fluxes in each layer and for the interface depth at the sill in Figs. 7 and 8. The observations of Sofianos et al. (2002) are included for comparison. Note that these observations are for, 1996 only, while our model forcings are for a 'typical' annual cycle.

Figs. 7 and 8 illustrate that model simulations are in good agreement with the observations of Sofianos et al. (2002) for the entire annual cycle. Quantitatively, both the layer depths at the sill and the exchange fluxes are accurately reproduced.

Qualitatively, the influx of the intermediate layer is clear from the model, showing an evolution with respect to time similar to the observations. The model fluxes are relatively steady during the winter regime and start to change over time significantly only after the summer regime commences. The intermediate layer 'opens up' at about the right time of year. The flux in the lower layer during summer drops to about 10% of its winter value, and the upper layer flux reverses, in agreement with observations (Sofianos et al., 2002).

The presence of abrupt changes in the model solutions through the annual cycle is clear (Fig. 9). The characteristic solutions during different periods are described as solution types (Smeed, 2000) and result from the presence, or lack of, controls at the 'exits' and whether the flow consists of two or three layers. We find four solution types over the annual cycle. These are labelled A to D on Fig. 9. Type A represents a two-layer sub-maximal solution with a single control at the sill. With only two layers present at the sill both modes are controlled. Type B is a period of three-layer influence but with no intermediate layer present at the sill. In this period both the internal wave modes are controlled. Type C is a solution period where the intermediate layer is present but with no flux. In this case only the second mode is controlled. This situation is similar to those studied by Engqvist (1996), who analysed multi-layer exchange flows with one stagnant layer. Only the second mode is controlled. Type D represents the summer sub-maximal three-layer exchange with controls present at the sill and at the Red Sea 'exit'. Again only the second mode is controlled.

These general solution types are the same as those found and described by Smeed (2000) for his rectangular bathymetry (see his Fig. 10). Although in that case the equations were solved along the whole channel, the driving parameters were very similar to those used here. However, despite using similar driving parameters and finding the same solution types, Smeed (2000) did not achieve a satisfactory quantitative simulation of the annual cycle. The key difference between the present model and the earlier study (Smeed, 2000) lies in use of a non-rectangular

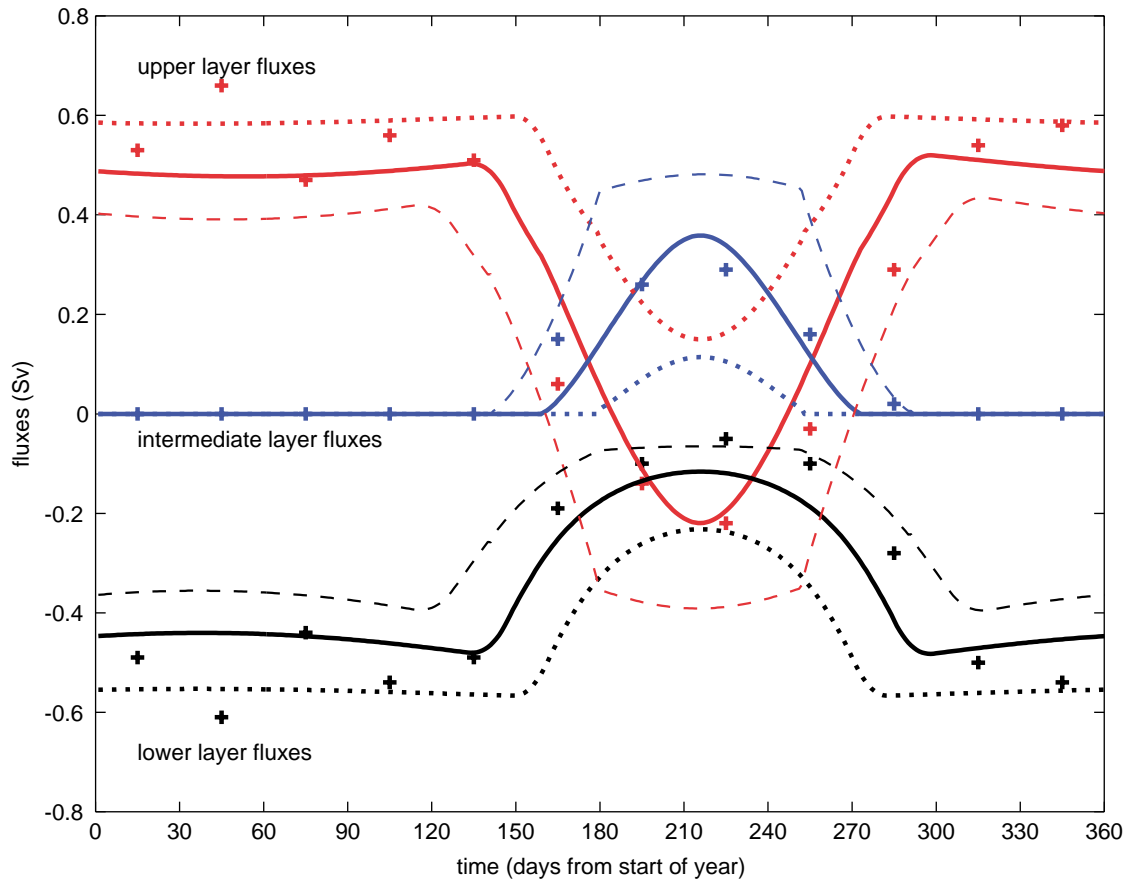


Fig. 7. Modelled fluxes in the various layers at the Bab el Mandab. According to uncertainties in the values used to force the model — is the best estimate (values used to drive the model are shown in Fig. 6), --- is the minimum estimate ( $r$  varies between 0.44 and 0.71, evaporation varies between 1.62 and 3.02  $\text{m yr}^{-1}$ , the Red Sea interface is set at 45 m, the Gulf of Aden interface varies between 15 and 105 m) and ····· is the maximum estimate generated by the model ( $r$  varies between 0.56 and 0.62, evaporation varies between 1.18 and 2.58  $\text{m yr}^{-1}$ , the Red Sea interface is set at 35 m, the Gulf of Aden interface varies between 25 and 115 m). The phases for the model drivers are the same as those shown in Fig. 6. Observations published by Sofianos et al. (2002) are marked by a +.

bathymetry, which results in a significantly improved approximation to the observed values of the exchange fluxes.

In contrast to our model the analysis of observations by Pratt et al. (1999, 2000) suggests that the flow at Hannish Sill is generally subcritical and only intermittently critical in both modes. Pratt et al. (1999) suggest that friction may be responsible for shifting the control point downstream of the sill. In this case our model would suggest that such a shift should not be so

substantial as to strongly affect the channel width and depth at the control. Pratt et al. (2000) suggest that control may be intermittent at the sill because of tides.

### 3.2. Sensitivity of the model

Given that the present model shows a sub-maximal exchange throughout the year, a high degree of model sensitivity to the driving parameters is to be expected. Our sensitivity tests show

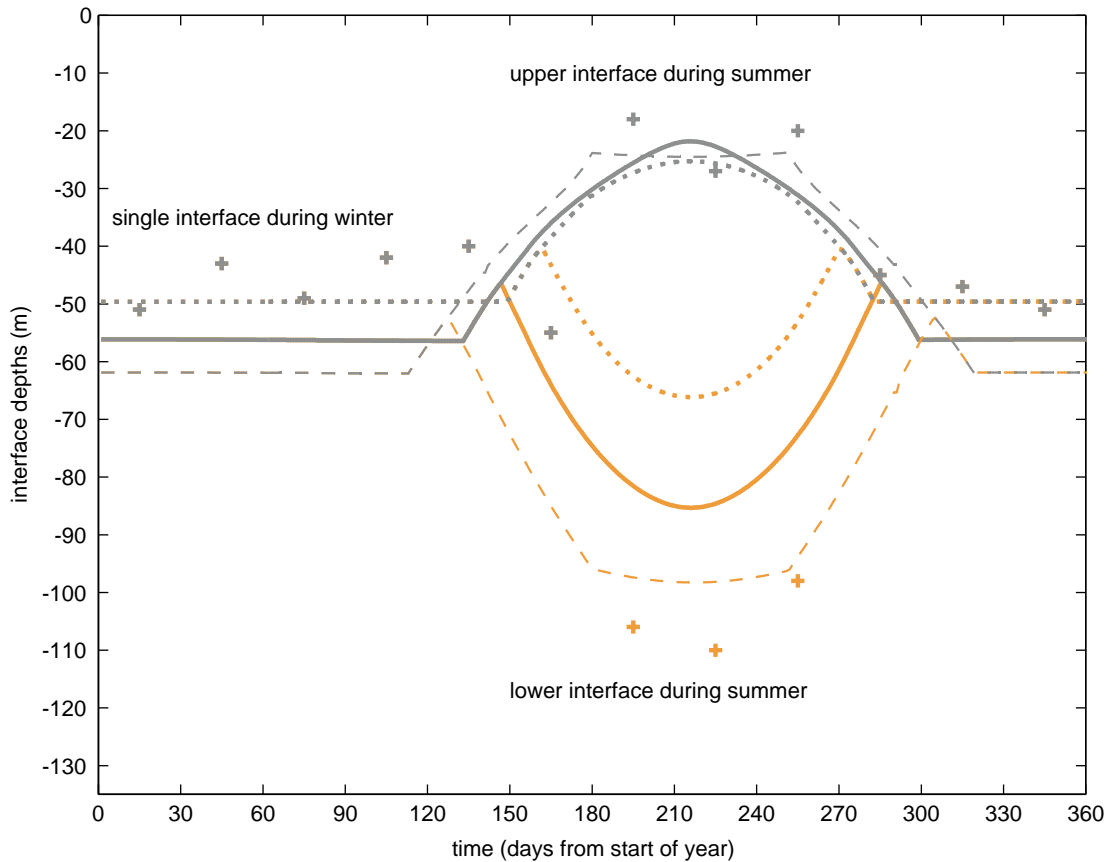


Fig. 8. Modelled interface depths for the various layers at Hanish Sill. According to uncertainties in the values used to force the model — is the best estimate (values used to drive the model are shown in Fig. 6), ---- is the minimum estimate ( $r$  varies between 0.44 and 0.71, evaporation varies between 1.62 and 3.02  $\text{m yr}^{-1}$ , the Red Sea interface is set at 45 m, the Gulf of Aden interface varies between 15 and 105 m) and ····· is the maximum estimate generated by the model ( $r$  varies between 0.56 and 0.62, evaporation varies between 1.18 and 2.58  $\text{m yr}^{-1}$ , the Red Sea interface is set at 35 m, the Gulf of Aden interface varies between 25 and 115 m). The phases for the model drivers are the same as those shown in Fig. 6. Observations published by Sofianos et al. (2002) are marked by a +. Observations published by Pratt et al. (1999) are marked by a +.

that the model is indeed sensitive to changes in the interface heights in each reservoir and  $r$ , but that it is not very sensitive to variations in the evaporative flux. Given the uncertainty in estimating the evaporative flux the sensitivity of the model fluxes to each is  $\sim \pm 0.2\%$ . This sensitivity is barely discernable in Figs. 10a and 11a. Interestingly when  $r$  is kept constant throughout the year, as in Fig. 10a, the midwinter minimum flux is lost and is replaced by a maximum flux. This indicates

that it is the low winter value of  $r$  that drives the midwinter minimum flux.<sup>1</sup>

Figs. 10b and 11b show the sensitivity of the model to the uncertainty in  $r$ . The uncertainty in the annually integrated flux is approximately 5%. This sensitivity is more significant over the summer period when it is as high as  $\pm 25\%$  (see Figs. 10b

<sup>1</sup>The density difference between GAIW and RSOW is constant so that  $g'(1-r)$  is constant as  $r$  varies.

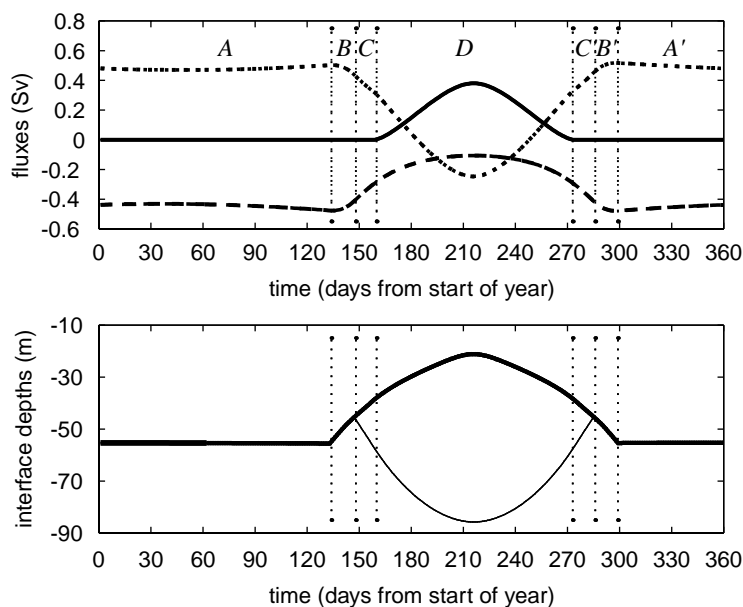


Fig. 9. The various stages of flow evolution as marked by the capital letters in the upper plot (see text for details). The forcing parameters used here are those used for our best estimate in Figs. 7 and 8.

and 11b). For the rest of the year the sensitivity is  $\sim \pm 4\%$ . The seasonally biased influence of  $r$  on the sensitivity is due to the fact that  $r$  does not directly influence the exchange over the winter period. The small wintertime influence of  $r$  is due indirectly to the dependence of the relative gravity between GASW and RSOW on  $r$ . Interestingly the upper and middle layers are more sensitive to variations in  $r$  than the lower layer by a factor of 3.

The influence of the uncertainty in the Gulf of Aden interface height (see Figs. 10c and 11c) is similar to the influence of  $r$ . This is because the Gulf of Aden interface height is significant only during the period of GAIW intrusion into the strait. The annually integrated exchange is affected by  $\pm 10\%$  given an uncertainty of  $\pm 5$  m in the interface height. This is maximum at the peak of the GAIW intrusion when the sensitivity approaches  $\sim \pm 30\%$ . The upper and middle layers are  $\sim 3$  times more sensitive to variations in the Gulf of Aden interface height than the lower layer.

A problem results from the large uncertainty in estimating the Red Sea interface height. The difference between the maximum and minimum

predictions is due to the uncertainties involved in assigning interface depths. Comparing Figs. 10 and 11 with Figs. 7 and 8 it is clear that much of the overall model uncertainty is due to uncertainty in estimating the Red Sea interface height. The annually integrated model sensitivity is approximately  $\pm 20\%$ . This sensitivity is steady throughout the year and is equivalent for each of the three layers. This uncertainty could be overcome by the incorporation of direct observations of the Red Sea interface depth throughout the year, if and when available in the future.

The model is less successful in reproducing wintertime fluxes and sill interface depths than summertime fluxes (Fig. 7). The interface is deeper than observed and the magnitude of the exchange fluxes is lower than observed over winter. The maximum prediction is driven with a Red Sea interface depth of 35 m and gives wintertime sill interface depths and fluxes closer to the observed values (dotted line in Fig. 7). The maximum prediction, however, represents a state of maximal exchange, so this observation does not automatically indicate that 35 m is a better Red Sea

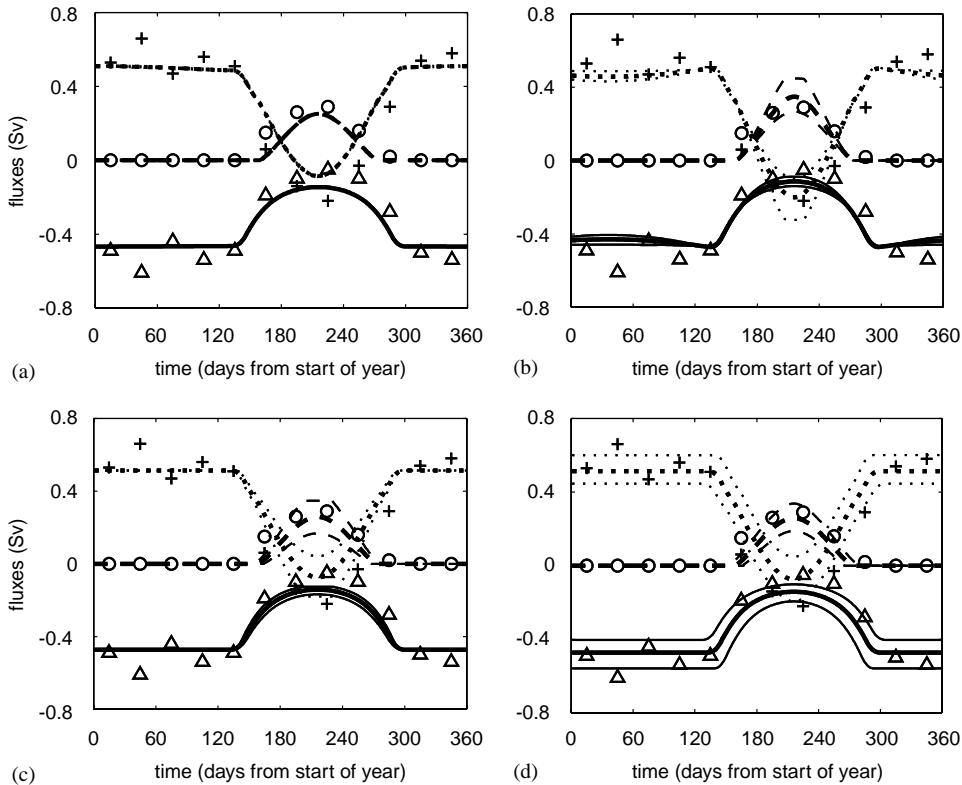


Fig. 10. Sensitivity of the model layer fluxes to the drivers:  $\cdots$  upper layer,  $---$  middle layer and  $—$  lower layer. The best estimate is the thick line and the maximum/minimum estimates are the thin lines. Observations of fluxes from Sofianos et al. (2002) for upper (+), middle (O) and lower layers ( $\Delta$ ) are also shown. Unless otherwise stated the Gulf of Aden interface is varied between 20 and 110 m and the other model drivers are kept constant at 40 m for the Red Sea interface,  $2.03 \text{ m yr}^{-1}$  for the evaporation and 0.58 for  $r$ . The phase of non-constant drivers is as in Fig. 6: (a) model sensitivity to evaporation which is given the values  $1.62\text{--}3.02$ ,  $1.4\text{--}2.8$  and  $1.18\text{--}2.58 \text{ m yr}^{-1}$ ; (b) model sensitivity to  $r$  which is given the values  $0.56\text{--}0.59$ ,  $0.5\text{--}0.65$  and  $0.44\text{--}0.71$ ; (c) model sensitivity to the evaporative flux which is given the values  $25\text{--}115$ ,  $20\text{--}110$  and  $15\text{--}105 \text{ m}$ ; (d) model sensitivity to the Red Sea interface, which is kept constant at 45, 40 and 35 m.

interface depth to use in the model: it could be deeper than this value. The model may therefore indicate that the wintertime exchange is fully maximal. As previously noted the interface depth in the Red Sea is not well known. The model result suggests that it is shallower than 40 m and probably closer to 35 m, when the exchange is only just submaximal, at least over the winter period.

The lower interface depth at the sill during the summer regime is also poorly reproduced (Fig. 7). This combined with the constant offset between the model and observations in the summertime

lower layer flux is again likely to be linked to the problem in estimating the Red Sea interface depth, although in this case indicating a deeper interface over summer. We have assumed that there is no seasonal variation in the Red Sea interface depth, but the discussion above would indicate that a value of 35 m is most suitable for the winter period along with a corresponding value of 45 m for the summer period. This would raise the wintertime interface depth at the sill (with a corresponding increase in the exchange flux) and lower it in summertime (with a corresponding decrease in the lower layer flux). Increasing  $r$  or making the Gulf

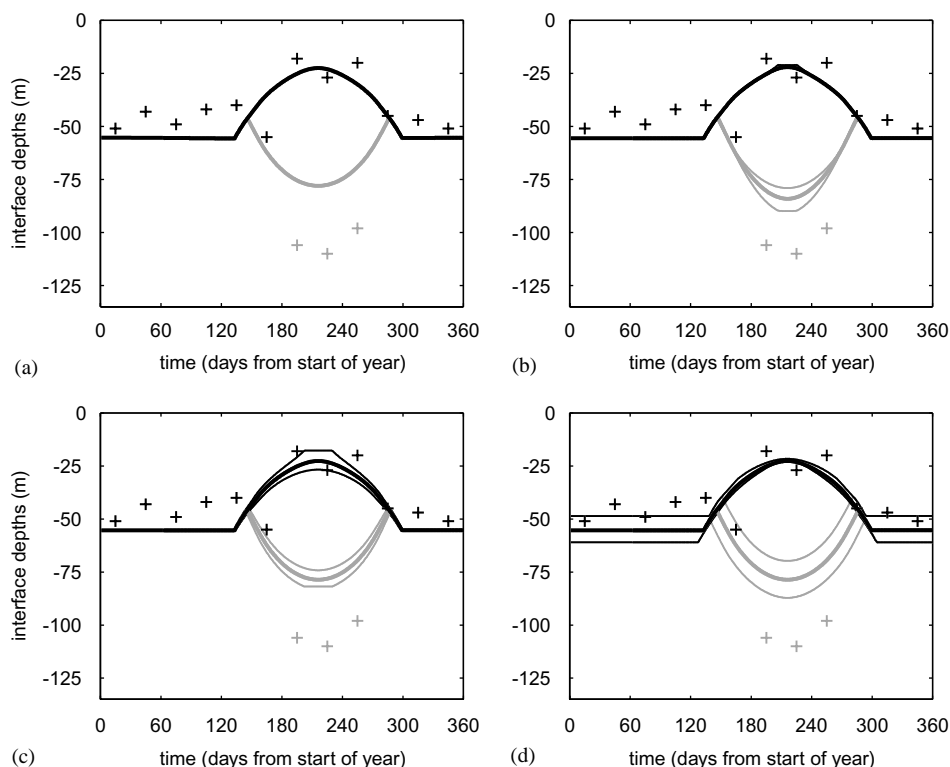


Fig. 11. Sensitivity of the model generated upper (black) and lower (grey) interface depths at Hannish Sill to the drivers. The best estimate is the thick line and the maximum/minimum estimates are the thin lines. Observations from Sofianos et al. (2002) are shown with a plus. Unless otherwise stated the Gulf of Aden interface is varied between 20 and 110 m and the other model drivers are kept constant at 40 m for the Red Sea interface,  $2.03 \text{ m yr}^{-1}$  for the evaporation and 0.58 for  $r$ . The phase of non-constant drivers is as in Fig. 6: (a) model sensitivity to the evaporation which is given the values 1.62–3.02, 1.4–2.8 and 1.18–2.58  $\text{m yr}^{-1}$ ; (b) model sensitivity to  $r$  which is given the values 0.56–0.59, 0.5–0.65 and 0.44–0.71; (c) model sensitivity to the evaporative flux which is given the values 25–115, 20–110 and 15–105 m; (d) model sensitivity to the Red Sea interface, which is kept constant at 45, 40 and 35 m.

of Aden interface depth shallower over the summer months would also deepen the lower interface in the summer but have no strong effect on the lower layer flux or on the upper interface in winter (see Figs. 10b,c and 11b,c). Given that for the modern exchange the evaporation has little effect on the exchange and that  $r$  and the Gulf of Aden interface height are relatively well understood, we strongly suspect that model prediction will be improved by future studies of the Red Sea interface height.

The model suggests that the exchange is not currently maximal in either the summer or winter regime. If that is true, then the use of a box model to represent the Red Sea, which would be driven

by the sill exchange (Matthiesen, 2001), may give a better indication of the Red Sea interface height and so remove the need to state it explicitly.

#### 4. Robustness and potential application

##### 4.1. Validity of approximations

The accuracy of the model is a first indication that the applied approximations are valid. In the development of the Mediterranean maximal exchange model a decade of modifications to Bryden and Stommel's (1984) original work took place as

non-rectangular cross sections (Bormans and Garrett, 1989; Bryden and Kinder, 1991; Dalziel, 1992), rotation (Dalziel, 1990; Pratt and Lundberg, 1991), and dissipation were added (Bormans and Garrett, 1989). This progress is exemplified by comparison of Bryden and Stommel (1984) with Bryden et al. (1994). Although the model presented here is rather successful already in simulating observed exchange characteristics, there remains scope for similar modifications to those applied to the Mediterranean studies. Having here included realistic cross section shapes, we follow Smeed's (2000) assessment that the main improvements in the future could be expected from the inclusion of time-dependent forcing and rotation. However, for many applications with high degrees of uncertainty (for example in paleoceanography) such modifications are expected to offer improvements that fall well within the range of uncertainties, so that these applications are best served by a model of minimum complexity, i.e. our current model. For contemporary oceanographic studies, however, possible improvements to the model should be explored.

Pratt et al. (1999, 2000) or that the internal Rossby radii of the first two internal modes are  $\sim 18$  and  $\sim 12$  km. This is comparable to the width of the strait at Perim Narrows (18 km), but the Hanish Sill section is wider by a factor of six (110 km). It is, however, not immediately obvious that this should make rotation significant to the exchange, because of the form of the cross section with depth and the presence of islands in the cross section at the sill. The decreasing width of the channel with depth means that the interface at  $\sim 50$  m depth during winter at the sill is subject to a channel width of 30 km, or only a maximum of 10 km uninterrupted by islands. In summer the lower interface is at a depth of 110 m with a channel width of only 8 km while the upper interface at 20 m depth has a width of 90 km. We further note the lack of any significant slope in the cross strait isopycnals in the observations of (Neuman and McGill, 1962; Maillard and Soliman, 1986). Although we cannot rule out that rotation plays some role in the exchange, it is doubtful that this role is more significant than model sensitivity to uncertainties in, for

example, the interface depths in the two reservoirs.

#### 4.2. Applications

The observations fall within the bands of error found by varying the model's forcing parameters (Fig. 7). These results give us confidence in applying the model to the applications for which it was developed.

From the equation for the salinity budget in the basin the residual salinity from the model can be calculated.

$$\bar{\rho}\overline{Q_3\Delta S} = \bar{\rho}(\overline{Q_1S_1} + \overline{Q_2S_2} + \overline{Q_3S_3}), \quad (8)$$

where  $S_i$  is the layer salinity,  $\Delta S$  is a residual salinity ( $\Delta S \sim 0$ ), and  $\bar{\rho}$  is the mean density of the layers. Using values of the annually integrated exchange from Fig. 7, the densities and salinities from Smeed (1997) and our maximum and minimum flux values to calculate the error, we obtain an insignificant residual salinity as  $0.0 \pm 0.9$ . The large error is due to the range between the maximum and minimum model estimates.

The equation for the net heat flux over the basin is

$$\overline{F_T} = \frac{1}{A}c_p\bar{\rho}(\overline{Q_1T_1} + \overline{Q_2T_2} + \overline{Q_3T_3} + \overline{ET_s}), \quad (9)$$

where  $T_i$  is the layer temperature,  $c_p$  is the heat capacity of water ( $3986 \text{ J deg}^{-1} \text{ kg}^{-1}$ ),  $T_s$  is the surface temperature (in our case obtained from the National Oceanographic Data Centre) and  $\tau$  is the heat loss over the Red Sea. Note that the use of  $\bar{\rho}$  is consistent with our approximation that volume rather than mass is conserved. Using the layer temperatures from Smeed (2000), except the upper layer, which is from Sofianos et al. (2002), and the model generated layer fluxes we get an answer of  $11 \pm 10 \text{ W m}^{-2}$  for the annual net heat flux from the basin. Our large error is due to uncertainty in the flux estimates from the model. Despite this large error our estimate compares well with the Sofianos et al. (2002) result of  $11 \pm 5 \text{ W m}^{-2}$ . We note that these authors also generate a large error due to uncertainties in their flux estimates.

The model requires that there is no net volume flux through the strait. The calculations above show that the annual mean flux of salt through the strait calculated by the model is close to zero. The model does though predict a small net heat loss from the surface of the Red Sea, in agreement with previous studies by Tragou et al. (1999) and Sofianos et al. (2002). The data presented in Smeed (1997) suggest that the GAIW water that enters the Red Sea in summer is mixed into the upper layer in the autumn, and Smeed (1997) attributed this to wind induced mixing and convective mixing from the surface.

The model allows us to calculate the change in the annually averaged flux across the strait due to the intrusion of the third layer relative to an imaginary continual two-layer exchange. The model predicts that the intrusion of the third layer reduces the annually averaged outflux in the lower layer to approximately 74% of its effective two-layer exchange value. The upper layer influx (which reverses during the summer period) is reduced to 63% of its effective two-layer value. The discrepancy between these two fluxes is balanced by the influx of GAIW. If this is taken into account, the total influx is reduced to 76% of its effective two-layer value, which balances the change in outflux and the net evaporative flux.

The Red Sea outflow is a significant source of intermediate water to the Indian Ocean, similar—if on a smaller scale—to the role of the Mediterranean outflow to the Atlantic hydrography. Longer-term monitoring of the exchange at the sill would be useful to develop a better understanding of the intermediate-depth thermohaline circulation in the Indian Ocean. Given the sensitivity of the submaximal strait dynamics to the south-west monsoon, any monitoring of the sill exchange would provide a useful indicator of the monsoon strength.

The intrusion of the third layer (GAIW) into the Red Sea appears to be a robust feature of the exchange. It currently intrudes into the Red Sea when the driving interface height in the Gulf of Aden is  $<40$  m or  $\sim 0.3$  times the sill depth. In the model the shallowest interface depth in the Gulf of Aden used to force the GAIW intrusion is 20 m. Ignoring any variation in monsoonal strength,

Red Sea interface depth or change in the channel width with depth, a tentative first approximation can be made of the sea level position at which the intrusion commences. This is carried out by considering when the total depth at the sill = 20/0.3 m. This would suggest that the total sill depth would need to be about 70 m, and sea level would therefore be 65–70 m lower than today, a condition achieved around 10 500 years before present (Fairbanks, 1989). This method predicts too young an age of the three-layer exchange since the channel thins with depth. Smeed (2000), however, assumes a rectangular channel cross-section that more closely resembles the channel in the period following the Last Glacial Maximum (LGM). In the Smeed (2000) model the intrusion of GAIW into the Red Sea occurs when the interface height in the Gulf of Aden is  $\sim 0.5$  times the sill depth. According to this prediction the intrusion first commenced when the total depth at the sill = 20/0.5 m. So Smeed's model suggests that the sea level would be 95–100 m lower than today, a condition achieved around 12 500 years before present (Fairbanks, 1989). The two models then combine to provide upper and lower bounds on the age of the GAIW intrusion at 10 500–12 500 years before present. The upper layer flow reversal would also first occur at around that time. The question of basin adaptation to these changes and consequent feedback to the sill dynamics cannot be answered before inclusion of some form of basin representation (Matthiesen, 2001) in the present model.

Before three-layer exchange could be established, a two-layer system would have prevailed. The two-layer exchange at Bab el Mandab would have been maximal during periods of very low sea level since the LGM with the depth at the sill approaching 20 m (Fairbanks, 1989). The very limited exchange caused hypersaline (salinity  $>49$ ) conditions in the Red Sea, which engendered aplanktonic zones in the sediment record (Rohling, 1994; Rohling and Zachariasse, 1996; Fenton, 1998; Fenton et al., 2000). Note that even today the maximum flux during winter in Fig. 4 indicates that the modern exchange is still very close to maximal. Further analysis of the past exchange history with the model must await the incorporation of a box model. Such an extension to the

model would be able not only to predict when the exchange would become maximal in terms of sea level, but also to evaluate the time scales of basin adaptation to changing dynamics at the sill (Lane-Serff et al., 1997). At the present stage of development, however, the approach of Bryden and Kinder (1991) of combining a maximal exchange hypothesis with the Knudsen equations for salinity conservation is valid for the glacial–early postglacial period of maximal exchange, ignoring any frictional effects (Rohling, 1994; Rohling and Zachariasse, 1996; Rohling et al., 1998).

The flux predicted by the model for the present day is submaximal throughout the year. This means that it is sensitive to the interface depth in the Gulf of Aden in summer. The modern flux as calculated from current meter observations by Sofianos et al. (2002) is therefore a sensitive indicator of the present day south-west monsoon strength.

### Acknowledgements

Input from Gregory Lane-Serff was useful in developing many of the concepts used in this paper.

### Appendix A

The derivation of the control condition is given below:

Following Gill (1977) for single layer flows and Dalziel (1991) for two-layer flows,  $J$  and  $K$  can be regarded as functionals. Thus we are seeking solutions to

$$\mathbf{J}(b_3, q_1, q_2, q_3, H_1, H_2; d_1, d_2) = \begin{pmatrix} J \\ K \end{pmatrix} = 0. \quad (\text{A.1})$$

Solutions of (8) can be traced along the channel by solving

$$\begin{pmatrix} \frac{dJ}{dx} \\ \frac{dK}{dx} \end{pmatrix} = \begin{pmatrix} 0 \\ 0 \end{pmatrix}, \quad (\text{A.2})$$

which can be written as

$$\mathbf{M} \begin{pmatrix} \frac{dd_1}{dx} \\ \frac{dd_2}{dx} \end{pmatrix} = \mathbf{N} \begin{pmatrix} \frac{dd_3}{dx} \end{pmatrix}, \quad (\text{A.3})$$

where

$$\mathbf{M} = \begin{pmatrix} \frac{\partial J}{\partial d_1} & \frac{\partial J}{\partial d_2} \\ \frac{\partial K}{\partial d_1} & \frac{\partial K}{\partial d_2} \end{pmatrix}, \text{ and } \mathbf{N} = \begin{pmatrix} \frac{\partial J}{\partial d_3} \\ \frac{\partial K}{\partial d_3} \end{pmatrix}, \quad (\text{A.4})$$

When the flow is critical with respect to one or both of the modes,

$$\det(\mathbf{M}) = 0. \quad (\text{A.5})$$

(see, e.g., (Baines, 1988)). The determinant of  $\mathbf{M}$  is given as,

$$\det(\mathbf{M}) = \frac{\partial J}{\partial d_2} \frac{\partial K}{\partial d_1} - \frac{\partial J}{\partial d_1} \frac{\partial K}{\partial d_2}. \quad (\text{A.6})$$

which is equal to Eq. (7).

### Appendix B

The Bernoulli functionals and control conditions for the two exits are given below

$$J_S = \frac{1}{2} \left( \frac{q_1}{a_{1S}} \right)^2 - \frac{1}{2} \left( \frac{q_2}{a_{2S}} \right)^2 + rd_{1S} - H_1 = 0, \quad (\text{B.1})$$

$$K_S = \frac{1}{2} \left( \frac{q_2}{a_{2S}} \right)^2 - \frac{1}{2} \left( \frac{q_3}{a_{3S}} \right)^2 + d_{2S}(1-r) - H_2 = 0, \quad (\text{B.2})$$

$$F_{2S}^2 \left( F_{2S}^2 \frac{b_{1S}}{b_{2S}} \right) - \left( r - F_{1S}^2 - F_{2S}^2 \frac{b_{1S}}{b_{2S}} \right) \times \left( 1 - r - F_{2S}^2 - F_{3S}^2 \frac{b_{2S}}{b_{3S}} \right) = 0, \quad (\text{B.3})$$

$$J_{RS} = \frac{1}{2} \left( \frac{q_1}{a_{1RS}} \right)^2 - \frac{1}{2} \left( \frac{q_2}{a_{2RS}} \right)^2 + rd_{1RS} - H_1 = 0, \quad (\text{B.4})$$

$$K_{RS} = \frac{1}{2} \left( \frac{q_2}{a_{2RS}} \right)^2 + d_{2RS}(1-r) - H_2 = 0, \quad (\text{B.5})$$

$$F_{2RS}^2 \left( F_{2RS}^2 \frac{b_{1RS}}{b_{2RS}} \right) - \left( r - F_{1RS}^2 - F_{2RS}^2 \frac{b_{1RS}}{b_{2RS}} \right) \times (1-r - F_{2RS}^2) = 0, \quad (\text{B.6})$$

$$J_{GoA} = \frac{1}{2} \left( \frac{q_1}{a_{1GoA}} \right)^2 + r d_{1GoA} - H_1 = 0, \quad (\text{B.7})$$

$$r - F_{1GoA}^2 = 0, \quad (\text{B.8})$$

where the subscripts S, RS and GoA denote Hanish Sill, the Red Sea and Gulf of Aden, respectively.

## References

- Baines, P.G., 1988. A general method for determining upstream effects in stratified flow of finite depth over long two-dimensional obstacles. *Journal of Fluid Mechanics* 188, 1–22.
- Bormans, M., Garrett, C., 1989. The effects of non-rectangular cross section, friction and barotropic fluctuations on the exchange through the Strait of Gibraltar. *Journal of Physical Oceanography* 19, 1543–1557.
- Bormans, M., Garrett, C., Thompson, K.R., 1986. Seasonal Variability of the surface inflow through the Strait of Gibraltar. *Oceanologica Acta* 9, 403–414.
- Bryden, H.L., Kinder, T.H., 1991. Steady two-layer exchange through the Strait of Gibraltar. *Deep Sea Research* 38, 445–463.
- Bryden, H.L., Candela, J., Kinder, T.H., 1994. Exchange through the Strait of Gibraltar. *Progress in Oceanography* 33, 201–248.
- Bryden, H.L., Stommel, H.M., 1984. Limiting processes that determine the basic features of the circulation in the Mediterranean Sea. *Oceanologica Acta* 7 (3), 289–296.
- Cember, R.P., 1988. On the sources, formation and circulation of Red Sea Deep Water. *Journal of Geophysical Research* 93 (C7), 8175–8191.
- Cromwell, D., Smeed, D.A., 1998. Altimetric observations of sea level cycles near the Strait of Bab al Mandab. *International Journal of Remote Sensing* 19 (8), 1561–1578.
- Dalziel, S.B., 1990. Rotating two-layer sill flows. In: Pratt, L.J., (Ed.), *The Physical Oceanography of Sea Straits*. Kluwer Academic Press, Netherlands.
- Dalziel, S.B., 1991. Two-layer hydraulics: a functional approach. *Journal of Fluid Mechanics* 223, 135–163.
- Dalziel, S.B., 1992. Maximal exchange in channels with nonrectangular cross sections. *Journal of Physical Oceanography* 22, 1188–1206.
- Degens, E.T., Ross, D.A., 1969. *Hot Brines and Recent Heavy Metal Deposits in the Red Sea*. New York, Springer.
- Engqvist, A., 1996. Self-similar multi-layer exchange flow through a contraction. *Journal of Fluid Mechanics* 328, 49–66.
- Fairbanks, R.C., 1989. A 17,000 year glacio-eustatic sea level record: influence of glacial melting rates on the Younger Dryas event and deep ocean circulation. *Nature* 342, 637–642.
- Fenton, M., 1998. *Late Quaternary History of Red Sea Outflow*. School of Ocean and Earth Sciences. University of Southampton, Southampton.
- Fenton, M.S., Geiselhart, E., Rohling, J., Hemleben, C., 2000. A planktonic zones in the Red Sea. *Marine Micropaleontology* 40, 277–294.
- Gill, A.E., 1977. The hydraulics of rotating-channel flow. *Journal of Fluid Mechanics* 80 (4), 641–671.
- Hogg, N.G., 1983. Hydraulic control and flow separation in a multi layer fluid with applications to the Vema channel. *Journal of Physical Oceanography* 13, 695–708.
- Killworth, P.D., 1992. On hydraulic control in a stratified fluid. *Journal of Fluid Mechanics* 237, 605–626.
- Lane-Serff, G.F., Rohling, E.J., Bryden, H.L., Charnock, H., 1997. Postglacial connection of the Black Sea to the Mediterranean and its relation to the timing of sapropel formation. *Paleoceanography* 12 (2), 169–174.
- Lane-Serff, G.F., Smeed, D.A., Postlethwaite, C.R., 2000. Multi-layer hydraulic exchange flows. *Journal of Fluid Mechanics* 416, 269–296.
- Maillard, C., Soliman, G., 1986. Hydrography of the Red Sea and exchanges with the Gulf of Aden in summer. *Oceanologica Acta* 9 (3), 249–269.
- Matthiesen, S., 2001. The feedback between basin and strait processes in the Mediterranean Sea and similar marginal seas—a process study. Ph.D. Thesis, University of Edinburgh, Edinburgh.
- Morcos, S.A., 1970. Physical and chemical oceanography of the Red Sea. *Oceanography and Marine Biology Annual Review* 8, 73–202.
- Murray, S.P., Johns, W., 1997. Direct observations of seasonal exchange through the Bab el Mandab Strait. *Geophysical Research Letters* 24 (21), 2557–2560.
- Neuman, C.A., McGill, D., 1962. Circulation of the Red Sea in early summer. *Deep-Sea Research* 8, 223–235.
- Nielsen, J.N., 1912. Hydrography of the Mediterranean and adjacent Waters, in: *Report on the Danish Oceanographical Expeditions 1908–1910*, 1, 1199–1223.
- Pratt, L.J., Lundberg, P.A., 1991. Hydraulics of rotating strait and sill flow. *Annual Review of Fluid Mechanics* 23, 81–106.
- Pratt, L.J., Johns, W., Murray, S.P., Katsumata, K., 1999. Hydraulic interpretation of direct velocity measurements in the Bab el Mandab Strait. *Journal of Physical Oceanography* 29, 2769–2784.
- Pratt, L.J., Deese, H.E., Murray, S.P., Johns, W., 2000. Continuous dynamical modes in straits having arbitrary cross sections with applications to the Bab el Mandab. *Journal of Physical Oceanography* 30, 2515–2534.

- Rohling, E.J., 1994. Glacial conditions in the Red Sea. *Paleoceanography* 9 (5), 653–660.
- Rohling, E.J., Zachariasse, W.J., 1996. Red Sea outflow during the last glacial maximum. *Quaternary International* 31, 77–83.
- Rohling, E.J., Fenton, M., Jorissen, F.J., Bertrand, P., Gansen, G., Caulet, J.P., 1998. Magnitudes of sea-level lowstands of the past 500,000 years. *Nature* 394, 162–165.
- Smeed, D.A., 1997. Seasonal Variation of the flow in the strait of Bab el Mandab. *Oceanologica Acta* 20 (6), 773–781.
- Smeed, D.A., 2000. Hydraulic control of three-layer exchange flows: application to the Bab-al-Mandab. *Journal of Physical Oceanography* 30, 2574–2588.
- Sofianos, S.S., Johns, W., Murray, S.P., 2002. Heat and freshwater budgets in the Red Sea from direct observations at Bab el Mandab. *Deep-Sea Research II* 49 (7-8), 1323–1340.
- Tragou, E., Garrett, C., Outerbridge, R., Gilman, C., 1999. The heat and freshwater budgets of the Red Sea. *Journal of Physical Oceanography* 29, 2504–2522.
- Werner, F., Lange, K., 1975. A bathymetric survey of the sill area between the Red Sea and the Gulf of Aden. *Geologisches Jahrbuch D* 13, 125–130.
- Winter, A., Almogi-Labin, A., Erez, Y., Halicz, E., Luz, B., Reiss, S., 1983. Salinity tolerance of marine organisms deduced from Red Sea Quaternary record. *Marine Geology*, M17–M22.